# An Uncertain Optimal Energy Flow Model for CCHP Campus Microgrid Using Parameterized Probability Boxes

Shunjiang Lin, *Senior Member*, *IEEE*, Xuan Sheng, Yuquan Xie, Yanghua Liu, and Mingbo Liu, *Member*, *IEEE*

***Abstract*—Due to the uncertain fluctuations of renewable energy and load power, the state variables such as bus voltages and pipeline mass flows in the combined cooling, heating, and power campus microgrid (CCHP-CMG) may exceed the secure operation limits. In this paper, an optimal energy flow (OEF) model for a CCHP-CMG using parameterized probability boxes (*p*-boxes) is proposed to describe the higher-order uncertainty of renewables and loads. In the model, chance constraints are used to describe the secure operation limits of the state variable *p*-boxes, and variance constraints are introduced to reduce their random fluctuation ranges. To solve this model, the chance and variance constraints are transformed into the constraints of interval cumulants (ICs) of state variables based on the *p*-efficient point theory and interval Cornish-Fisher expansion. With the relationship between the ICs of state variables and node power, and using the affine interval arithmetic method, the original optimization model is finally transformed into a deterministic nonlinear programming model. It can be solved by the CONOPT solver in GAMS software to obtain the optimal operation point of a CCHP-CMG that satisfies the secure operation requirements considering the higher-order uncertainty of renewables and loads. Case study on a CCHP-CMG demonstrates the correctness and effectiveness of the proposed OEF model.**

***Index Terms*—Combined cooling, heating, and power campus microgrid (CCHP-CMG), chance-constrained programming, higher-order uncertainty, optimal energy flow, parameterized probability box.**

## NOMENCLATURE

*A. Parameters*

| | |
|---|---|
| $\alpha_{\mathrm{mh/c,min}}$, $\alpha_{\mathrm{mh/c,max}}$ | Confidence levels that mass flow meets lower and upper secure limit constraints |
| $\alpha_{\mathrm{Tsh,min}}$, $\alpha_{\mathrm{Tsc,max}}$ | Confidence levels that heating/cooling supply temperature meets constraints |
| $\alpha_{U,\mathrm{min}}$, $\alpha_{U,\mathrm{max}}$ | Confidence levels that voltage amplitude meets lower and upper limit constraints |
| $\Gamma(x)$ | Gamma function |
| $\zeta(\cdot)$ | Inverse cumulative distribution function (CDF) of standard normal distribution |
| $\boldsymbol{\eta}_{\mathrm{HE}}$, $\boldsymbol{\eta}_{\mathrm{AC}}$ | Efficiency coefficients of heat exchange unit and absorption chiller |
| $\boldsymbol{\eta}_{\mathrm{HP}}$, $\boldsymbol{\eta}_{\mathrm{EC}}$ | Efficiency coefficients of heat pumps and electric chillers |
| $\eta_{\mathrm{PV}}$, $\eta_{\mathrm{PT}}$ | Efficiency factors of photovoltaic (PV) and photothermic (PT) stations |
| $\theta_{\mathrm{PV}}$ | Power factor angle of PV station |
| $[\boldsymbol{\theta}]$ | Vector of distribution parameter intervals |
| $\underline{\boldsymbol{\theta}}$, $\bar{\boldsymbol{\theta}}$ | Lower and upper bounds of $[\boldsymbol{\theta}]$ |
| $[\mu_{\mathrm{L}}]$, $[\sigma_{\mathrm{L}}^2]$ | Uncertainty interval of $\mu_{\mathrm{L}}$ and $\sigma_{\mathrm{L}}^2$ |
| $\underline{\mu}_{\mathrm{L}}$, $\bar{\mu}_{\mathrm{L}}$ | Lower and upper bounds of interval $[\mu_{\mathrm{L}}]$ |
| $\sigma_{U,\max}^2$, $\sigma_{\mathrm{mh,max}}^2$, $\sigma_{\mathrm{mc,max}}^2$, $\sigma_{\mathrm{Tsh,max}}^2$, $\sigma_{\mathrm{Tsc,max}}^2$ | Upper limits of the central values of variance intervals of $U_i$, $m_{hi}$, $m_{ci}$, $T_{shi}$, $T_{sci}$ |
| $\underline{\sigma}_{\mathrm{L}}^2$, $\bar{\sigma}_{L}^2$ | Lower and upper bounds of interval $[\sigma_{\mathrm{L}}^2]$ |
| $\boldsymbol{\Phi}_{\mathrm{G}i,\mathrm{h/c,min}}$, $\boldsymbol{\Phi}_{\mathrm{G}i,\mathrm{h/c,max}}$ | Lower and upper limits of heating/cooling power output of combined cooling, heating, and power (CCHP) unit at node $i$ |
| $a_{1i}$-$a_{5i}$ | Cost coefficients of CCHP unit |
| $A_{\mathrm{PV}}$, $A_{\mathrm{PT}}$ | Areas of PV and PT panels |
| $\boldsymbol{A}_{\mathrm{h/c}}$ | Network incidence matrix of heating/cooling network |
| $\boldsymbol{B}_{\mathrm{h/c}}$ | Loop incidence matrix of heating/cooling network |

Manuscript received: August 24, 2022; revised: November 27, 2022; accepted: January 20, 2023. Date of CrossCheck: January 20, 2023. Date of online publication: March 7, 2023.

This work was supported by the National Natural Science Foundation of China (No. 51977080) and the Natural Science Foundation of Guangdong Province (No. 2022A1515010332).



S. Lin (corresponding author), X. Sheng, and M. Liu are with the School of Electric Power Engineering, South China University of Technology, Guangzhou 510640, China (e-mail: linshj@scut.edu.cn; 601911447@qq.com; epmbliu@scut.edu.cn).

Y. Xie is with the Digital Grid Research Institute, China Southern Power Grid, Guangzhou 510700, China (e-mail: 605150928@qq.com).

Y. Liu is with the School of Electromechanical Engineering, Guangdong Polytechnic Normal University, Guangzhou, China (e-mail: 1148972539@qq.com).

DOI: 10.35833/MPCE.2022.000536

$c_{DN}$ Unit power purchase price

$c_w$ Specific heat capacity of water

$c(\cdot)$ Cornish-Fisher expansion function

$\boldsymbol{C}_G$ Heat-to-power ratio of CCHP unit

$F_{WL}(\cdot)$ CDF of load power (obeys normal distribution)

$F_{WR}(\cdot)$ CDF of solar irradiance (obeys beta distribution)

$F_X(\cdot)$ CDF of random variable $X$

$G_{ij}$, $B_{ij}$ Real and imaginary parts of the $i^{th}$ row and $j^{th}$ column element of node admittance matrix

$\boldsymbol{K}$ Resistance coefficient of pipeline

$[p_\alpha]$, $[p_\beta]$ Uncertain intervals of $p_\alpha$ and $p_\beta$

$\underline{p}_\alpha$, $\bar{p}_\alpha$ Lower and upper bounds of $[p_\alpha]$

$\underline{p}_\beta$, $\bar{p}_\beta$ Lower and upper bounds of $[p_\beta]$

$P_{Gi,min}$, $P_{Gi,max}$ Lower and upper limits of active power output of CCHP unit at bus $i$

$s$ Mark of heating/cooling network (1 or −1 represents heating or cooling network, respectively)

$S_G$ Set of CCHP unit access nodes

$T_a$ Ambient temperature

$T_{Gi,h/c,min}$, $T_{Gsi,h/c,max}$ Lower and upper limits of heating/cooling supply temperature of CCHP unit at node $i$

$T_{shi,min}$, $T_{sci,max}$ Lower limit of heating supply temperature and upper limit of cooling supply temperature at load node $i$

$U_{Gi,min}$, $U_{Gi,max}$ Lower and upper limits of terminal voltage of CCHP unit at bus $i$

$U_{i,min}$, $U_{i,max}$ Lower and upper limits of the voltage amplitude at bus $i$

$w_{Rmax}$ The maximum solar irradiance

*B. Variables*

$[\boldsymbol{\gamma}^{(k)}_{\Delta Pe}]$, $[\boldsymbol{\gamma}^{(k)}_{\Delta Qe}]$, $[\boldsymbol{\gamma}^{(k)}_{\Delta \Phi h}]$, $[\boldsymbol{\gamma}^{(k)}_{\Delta \Phi c}]$ The $k^{th}$-order interval cumulant (IC) vectors of fluctuations of active power load, reactive power load, heating load, and cooling load

$[\gamma^{(2)}_{Ui}]$, $[\gamma^{(2)}_{mhi}]$, $[\gamma^{(2)}_{mci}]$, $[\gamma^{(2)}_{Tshi}]$, $[\gamma^{(2)}_{Tsci}]$ The 2nd-order ICs of $U_i$, $m_{hi}$, $m_{ci}$, $T_{shi}$, $T_{sci}$

$\gamma^{(k)}_X$, $[\gamma^{(k)}_X]$ The $k^{th}$-order cumulant and IC of output random variable $X$

$\gamma^{(2)}_{X,0}$, $\gamma^{(2)}_{X,1}$ Central value and the 1st-order partial derivative of $\hat{\gamma}^{(2)}_X$

$\delta_{ij}$ Voltage phase angle difference between bus $i$ and bus $j$

$\varepsilon_i$ The $i^{th}$ independent noise element of $u$

$\boldsymbol{\mu}_L$, $\boldsymbol{\sigma}^2_L$ Mean and variance of load power $w_L$

$\sigma_X$, $[\sigma_X]$ Standard deviation and standard deviation interval of output random variable $X$

$\sigma_{X,0}$, $\sigma_{X,1}$ Central value and the 1st-order partial derivative of $\hat{\sigma}_X$

$[\sigma^2_{Ui}]$, $[\sigma^2_{mhi}]$, $[\sigma^2_{mci}]$, $[\sigma^2_{Tshi}]$, $[\sigma^2_{Tsci}]$ Variance intervals of $U_i$, $m_{hi}$, $m_{ci}$, $T_{shi}$, $T_{sci}$

$\boldsymbol{\Phi}_{Gi}$ Waste heat output of CCHP unit

$\boldsymbol{\Phi}_{G,h}$, $\boldsymbol{\Phi}_{G,c}$ Heating and cooling power outputs of CCHP unit

$\boldsymbol{\Phi}_{h/c}$ Vector of heating/cooling power consumed at nodes

$\boldsymbol{\Phi}_{HP}$, $\boldsymbol{\Phi}_{EC}$ Power outputs of heat pump and electric chiller

$\boldsymbol{\Phi}_H$, $\boldsymbol{\Phi}_C$ Waste heat power of CCHP units for heating and cooling

$\boldsymbol{\Phi}_{L,h}$, $\boldsymbol{\Phi}_{L,c}$ Heating and cooling load power

$\boldsymbol{\Phi}_{PT}$ Power output of PT station

$C_{CCHP}$ Operation cost of CCHP unit

$C_{DN}$ Cost of power purchased by distribution network

$F^{-1}_{Ui}(\cdot)$, $F^{-1}_{mhi}(\cdot)$, $F^{-1}_{mci}(\cdot)$, $F^{-1}_{Tshi}(\cdot)$, $F^{-1}_{Tsci}(\cdot)$ Inverse CDF functions of $U_i$, $m_{hi}$, $m_{ci}$, $T_{shi}$, $T_{sci}$

$[g_k]$ The $k^{th}$-order normalized IC of $X$

$g_i$ The $i^{th}$-order normalized cumulant of $X$

$\boldsymbol{m}_{h/c}$ Vector of mass flows within pipes of heating/cooling network

$m_{in}$, $m_{out}$ Mass flows within a pipe leaving and coming from node

$\boldsymbol{m}_{q,h/c}$ Vector of mass flows at heating/cooling nodes

mid$(\cdot)$ Central value of an interval

$p_\alpha$, $p_\beta$ Shape parameters of beta distribution

$P_{DN}$ Active power injected by distribution network

$P_{Gi}$, $Q_{Gi}$ Active and reactive power outputs of CCHP unit

$P_{HPi}$, $P_{ECi}$ Electricity power consumed by heat pump and electric chiller at bus $i$

$P_{Li}$, $Q_{Li}$ Load power at bus $i$

$P_{PVi}$, $Q_{PVi}$ Active and reactive power outputs of PV station at bus $i$

sup$(\cdot)$ Upper bound of an interval

$\boldsymbol{S}$ Sensitivity matrix of state variables with respect to node power

$\boldsymbol{T}_{sh/c}$, $\boldsymbol{T}_{rh/c}$ Vectors of supply and return temperatures

| | |
|---|---|
| $T_{start}$, $T_{end}$ | Temperatures at start and end nodes of a pipe |
| $T_{in}$, $T_{out}$ | Temperatures at inflow and outflow nodes |
| $\hat{u}$ | Affine form of $u$ |
| $u_0$ | Central value of $u$ |
| $u_i$ | The $i^{th}$ partial derivative of $u$ |
| $U_i$ | Voltage magnitude at bus $i$ |
| $w_L$, $w_R$ | Load power and solar irradiance |
| $x$ | Deterministic variables |
| $X^P$ | Parameterized $p$-box |
| $Z$ | Random variables |

*C. Subscripts*

| | |
|---|---|
| $(\cdot)_c$ | Variables of cooling network |
| $(\cdot)_G$ | Variables of CCHP unit |
| $(\cdot)_h$ | Variables of heating network |

## I. Introduction

In a combined cooling, heating and power campus microgrid (CCHP-CMG), except for supplying electrical loads, the waste heat from the CCHP unit is used for supplying cooling/heating loads, which can improve the efficiency of energy utilization. In addition, the accommodation capacity of renewable energy can be improved by the complementary operation of multiple energies of cooling, heating, and electricity in the microgrid. Thus, CCHP-CMGs have been widely applied in the energy supply of emerging industrial campuses in recent years [1], [2]. In order to further improve the secure and economic operation of the system, the optimal energy flow (OEF) calculation model is usually established to search the optimal operation point of the system. However, there are uncertain fluctuations in the renewable energy output and load power in the CCHP-CMG, which have harmful effects on its secure operation. Therefore, it is of vital importance to take into account the uncertainty in the OEF calculation, which has been widely discussed in the existing literature.

Currently, the most commonly used methods in the OEF calculation considering the uncertainty include the stochastic programming method, robust optimization (RO) method, interval optimization method, and information gap decision theory (IGDT). In [3] and [4], the uncertain variables were described by uncertainty and ambiguity sets, and the OEF problems in gas-power systems were solved by robust optimization and distributionally robust optimization (DRO) methods. References [5] and [6] adopted interval optimization method to solve the OEF models considering the uncertainty, where the uncertain variables were described as intervals. Similar to the interval optimization method, IGDT is another non-probabilistic decision-making method. It includes risk-averse and risk-seeking strategies [7]. Reference [7] adopted both risk-averse and risk-seeking IGDT methods to the optimal bidding problem of electric vehicles. Reference [8] developed a multi-objective chance-constrained IGDT model to ensure the secure operation of distribution network. However, these three methods have their shortcomings. The RO method tends to focus on the most extreme scenario, and the optimization results are usually conservative, and the economics of the system operation is poor. For the interval optimization method, the uncertain variables are only modeled by their upper and lower bounds, ignoring the probabilistic distribution information inside the intervals, and the statistical information in the historical data of uncertain variables cannot be fully utilized. The IGDT framework is very conservative and may lead to over-estimated actions [9]. It is more suitable for the uncertainty where the statistical information in the historical data is limited [10]. In the stochastic programming method, the uncertain variables are described as random variables that obey the given probability distributions. In [11] and [12], the scenario method, a type of stochastic programming method, was used to deal with uncertainties of load power and renewable energy sources in the OEF models of multi-energy systems, where a large number of scenarios were generated and the scenario reduction methods were applied. However, it is time consuming to solve the large-scale multiple scenario optimization model. The chance-constrained programming (CCP) method is another type of stochastic programming method, which makes decisions by setting acceptable confidence levels of chance constraints (CCs). Reference [13] developed the optimal scheduling model for community-integrated energy systems, where spinning reserves were constructed in the form of CCs, considering the uncertainty of multiple renewable energy sources. Reference [14] used CCs to address the uncertainty problem caused by variable wind and solar power generation as well as load forecast errors, and developed a decentralized operation optimization model for an integrated power-gas system. Obviously, by adjusting the given confidence levels of CCs, the CCP method can achieve a trade-off between system reliability and economy and obtain a more flexible decision.

In the above-mentioned publications on the stochastic programming method, probabilistic models are used to describe the uncertainty of random variables, and the accuracy of probabilistic models will directly affect the effectiveness of the decision. However, the distribution parameters of probabilistic models are usually derived from historical data, hence it is difficult to obtain the accurate distribution parameters due to data loss, measurement errors, etc. The uncertainty of the distribution parameters of probabilistic models is called the higher-order uncertainty, which is a valuable issue in the optimal power flow (OPF) and OEF studies [15], [16]. Reference [17] proposed a robust chance-constrained OPF model where wind power prediction errors were assumed to obey a normal distribution and ambiguity sets were constructed to describe the uncertainty of moments such as mean and variance. Moreover, the uncertainty of the type of probability distribution and the distribution parameters were considered in the ambiguity set in [18], [19], and the OPF model based on the DRO method was proposed. Most of the existing literature on the OPF problem considering the higher-order uncertainties uses the DRO method,

where the ambiguity set is constructed. However, the DRO method with moment-based ambiguity set has a complex computational process, which requires simplification of the optimization model and usually uses the linear models such as the DC power flow model adopted in [17], [18], and [20]. And it is difficult to deal with the complex nonlinear energy flow equations such as the hydraulic and thermal models of the heating/cooling network in the integrated energy system [21]. Currently, the higher-order uncertainties in the OEF of gas-electric integrated system were analyzed in [20], where the gas network model can be easily transformed into a linear model. But no publications have focused on the OEF considering higher-order uncertainty of a CCHP-CMG including the complex nonlinear heating/cooling network model. Therefore, in this paper, the CCs of probability boxes (*p*-boxes) of state variables are used to describe the secure operation limits, and the variance constraints (VCs) of *p*-boxes of state variables are introduced to reduce their random fluctuations, and an OEF calculation method for a CCHP-CMG is proposed.

This paper makes three contributions. ① The parameterized *p*-boxes are used to describe the higher-order uncertainty of renewables and loads, and an OEF model for a CCHP-CMG including the CCs and VCs of the *p*-boxes of state variables is proposed. The CCs of the state variable *p*-boxes are used to describe the secure operation limits, and the VCs are introduced to reduce the random fluctuations of the state variable *p*-boxes. ② The CCs and VCs of the *p*-boxes are transformed into the constraints of the interval cumulants (ICs) of state variables by the *p*-efficient point theory and the interval Cornish-Fisher expansion. With the relationship between the ICs of state variables and node power, and by the affine interval arithmetic, the original optimization model is transformed into a deterministic nonlinear programming model, which can be solved by the CONOPT solver. ③ In the case study of a CCHP-CMG, comparative results of deterministic OEF, traditional CCP-based OEF, and the proposed OEF considering the higher-order uncertainty demonstrate that the optimal operation point obtained by the proposed OEF can ensure that the *p*-boxes of state variables satisfy the secure operation requirement with reduced random fluctuations when considering the higher-order uncertainty of renewables and loads.

The remainder of this paper is organized as follows. Section II introduces the structure of a CCHP-CMG and the traditional CCP-based OEF model. Section III develops the OEF model of the CCHP-CMG including the CCs and VCs of *p*-boxes considering the higher-order uncertainty of renewables and loads. Section IV presents the solution method for the proposed OEF model. Section V shows the case study and result analysis. Section VI concludes this paper.

## II. Traditional OEF Model for a CCHP-CMG Based on Chance-constrained Programming

### A. Structure of a CCHP-CMG

The structure and multiple energy supply process of a CCHP-CMG is shown in Fig. 1, including the CCHP units (gas generators, absorption chillers, heat exchange units), heat pumps, electric chillers, photovoltaic (PV), and photothermic (PT) stations, and other components. Among them, CCHP units supply the electricity, heating, and cooling load demands of users in the CCHP-CMG, and the insufficient electricity, heating, and cooling load demands are supplemented by external distribution network, heat pumps, and electric chillers, respectively. Additionally, the PV/PT stations provide clean energy for electricity and heating loads in the CCHP-CMG [21], [22].

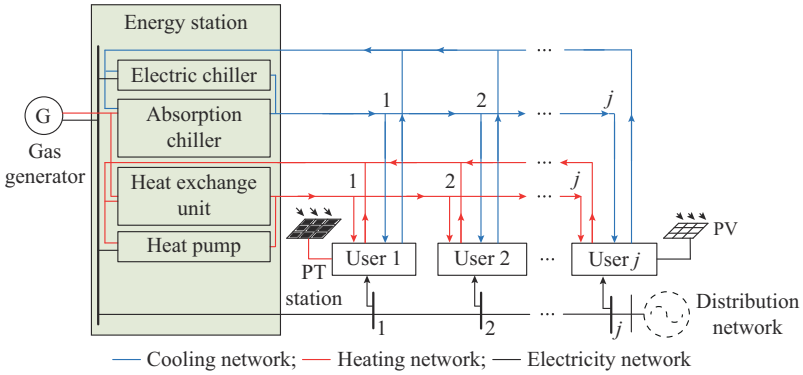


Fig. 1. Structure and multiple energy supply process of a CCHP-CMG.

### B. Traditional CCP-based OEF Model

#### 1) Objective Function

The objective of the traditional CCP-based OEF model is to minimize the total operation cost of the CCHP-CMG, as:

$$\min\left(C_{\mathrm{CCHP}}+C_{\mathrm{DN}}\right) \tag{1}$$

According to [23], the operation cost of the CCHP unit is given by:

$$C_{\mathrm{CCHP}}=\sum_{i\in S_G}\left(a_{5i}P_{\mathrm{G}i}\Phi_{\mathrm{G}i}+a_{4i}P_{\mathrm{G}i}^2+a_{3i}P_{\mathrm{G}i}+a_{2i}\Phi_{\mathrm{G}i}^2+a_{1i}\Phi_{\mathrm{G}i}+a_{0i}\right) \tag{2}$$

The power purchase cost from the external distribution network can be calculated by:

$$C_{\mathrm{DN}}=c_{\mathrm{DN}}P_{\mathrm{DN}} \tag{3}$$

#### 2) Operation Constraints

The electricity network operation constraints include the

power balance equation (4) and the active power output and terminal voltage limits of generators shown in (5).

$$\begin{cases} P_{Gi}-P_{HPi}-P_{ECi}-P_{Li}+P_{PVi}=U_i\sum_{j=1}^{n}U_j(G_{ij}\cos\delta_{ij}+B_{ij}\sin\delta_{ij}) \\ Q_{Gi}-Q_{Li}+Q_{PVi}=U_i\sum_{j=1}^{n}U_j(G_{ij}\sin\delta_{ij}-B_{ij}\cos\delta_{ij}) \end{cases} \tag{4}$$

$$\begin{cases} P_{Gi,\min}\le P_{Gi}\le P_{Gi,\max} \\ U_{Gi,\min}\le U_{Gi}\le U_{Gi,\max} \end{cases} \tag{5}$$

The operation characteristics of heating/cooling network include the hydraulic model and the thermal model. The hydraulic model includes the mass flow continuity equation (6) and loop pressure equation (7) [21].

$$\boldsymbol{A}_{h/c}\boldsymbol{m}_{h/c}=\boldsymbol{m}_{q,h/c} \tag{6}$$

$$\boldsymbol{B}_{h/c}\boldsymbol{K}\boldsymbol{m}_{h/c}\left|\boldsymbol{m}_{h/c}\right|=\boldsymbol{0} \tag{7}$$

The thermal model includes the power balance equation of nodes (8), the temperature drop equation of pipelines (9), and the temperature mixing equation of nodes (10) [21]. In (8), for the heating network, $\boldsymbol{\Phi}_h=\boldsymbol{\Phi}_{L,h}-(\boldsymbol{\Phi}_{G,h}+\boldsymbol{\Phi}_{HP}+\boldsymbol{\Phi}_{PT})$; for the cooling network, $\boldsymbol{\Phi}_c=\boldsymbol{\Phi}_{L,c}-(\boldsymbol{\Phi}_{G,c}+\boldsymbol{\Phi}_{EC})$.

$$\boldsymbol{\Phi}_{h/c}=c_w\boldsymbol{m}_{q,h/c}s(\boldsymbol{T}_{sh/c}-\boldsymbol{T}_{rh/c}) \tag{8}$$

$$T_{end}=(T_{start}-T_a)e^{-\frac{L}{mc_wR}}+T_a \tag{9}$$

$$\sum m_{in}T_{in}=\left(\sum m_{out}\right)T_{out} \tag{10}$$

In addition, to ensure the secure operation, the heating/cooling power output limits and the supply temperature limits of the CCHP units are also required, as shown in (11) and (12), respectively.

$$\Phi_{Gi,h/c,\min}\le\Phi_{Gi,h/c}\le\Phi_{Gi,h/c,\max} \tag{11}$$

$$T_{Gsi,h/c,\min}\le T_{Gsi,h/c}\le T_{Gsi,h/c,\max} \tag{12}$$

The relationship between waste heat and electric power output of the CCHP unit is shown as follows [21]:

$$\boldsymbol{C}_G=\boldsymbol{\Phi}_G/\boldsymbol{P}_G \tag{13}$$

The waste heat is transformed into heating and cooling energies by heat exchange units and absorption chillers, respectively, and the energy conversion relationships are shown as:

$$\begin{cases} \boldsymbol{\Phi}_G=\boldsymbol{\Phi}_H+\boldsymbol{\Phi}_C \\ \boldsymbol{\Phi}_{G,h}=\boldsymbol{\eta}_{HE}\boldsymbol{\Phi}_H \\ \boldsymbol{\Phi}_{G,c}=\boldsymbol{\eta}_{AC}\boldsymbol{\Phi}_C \end{cases} \tag{14}$$

Similarly, the energy conversion relationships of other energy coupling elements such as heat pumps or electric chillers are as follows:

$$\begin{cases} \boldsymbol{\Phi}_{HP}=\boldsymbol{\eta}_{HP}\boldsymbol{P}_{HP} \\ \boldsymbol{\Phi}_{EC}=\boldsymbol{\eta}_{EC}\boldsymbol{P}_{EC} \end{cases} \tag{15}$$

*3) Chance Constraints of State Variables*

When considering the uncertainty of load power and PV/PT power output, the state variables in the CCHP-CMG also have uncertainty. In the CCP-based OEF model, the CCs are used to describe the secure limits of uncertain state variables. The CCs of bus voltages are shown in (16), the CCs of pipeline mass flows are as (17), and the CCs of heating and cooling load node supply temperatures are as in (18) and (19), respectively.

$$\begin{cases} \Pr\{U_i\le U_{i,\max}\}\ge\alpha_{U,\max} \\ \Pr\{U_{i,\min}\le U_i\}\ge\alpha_{U,\min} \end{cases} \tag{16}$$

$$\begin{cases} \Pr\{m_{h/ci}\le m_{h/ci,\max}\}\ge\alpha_{mh/c,\max} \\ \Pr\{m_{h/ci,\min}\le m_{h/ci}\}\ge\alpha_{mh/c,\min} \end{cases} \tag{17}$$

$$\Pr\{T_{shi,\min}\le T_{shi}\}\ge\alpha_{Tsh,\min} \tag{18}$$

$$\Pr\{T_{sci}\le T_{sci,\max}\}\ge\alpha_{Tsc,\max} \tag{19}$$

where $\Pr\{\cdot\}$ is the probability function.

The traditional CCP-based OEF model is shown in (20). In this model, the decision variables include the electricity/heating/cooling power output, generator voltage, and supply temperature of CCHP units. The state variables include the bus voltages, pipeline mass flow rates, and node supply/return temperatures. The input random variables include the electricity/heating/cooling load power and the PV/PT power output. By solving the above model, the optimal operation point, which minimizes the total operation cost considering the uncertain node power, can be obtained.

$$\begin{cases} \min(C_{CCHP}+C_{DN}) \\ \text{s.t. (4)-(19)} \end{cases} \tag{20}$$

In the traditional CCP-based OEF model, the cumulative distribution functions (CDFs) or probability density functions (PDFs) are used to describe the random variables of uncertain node power. The distribution parameters in the CDFs or PDFs are definite values. However, when the CDFs or PDFs of random variables are obtained by the statistical analysis of historical data, due to the absence of some historical data and the errors of measurement instruments, there may be uncertainties in the distribution parameters of uncertain node power. The uncertainties of the distribution parameters in the CDFs or PDFs are called higher-order uncertainties [15], [16]. Thus, when considering the higher-order uncertainties of the random variables, the optimal operation point obtained by the traditional CCP-based OEF model may still have the risks that the state variables exceed the secure operation limits.

## III. OEF Model of CCHP-CMG Considering Higher-order Uncertainty of Renewables and Loads

The parameterized *p*-box model is used to describe the higher-order uncertainty of renewables and loads, and the OEF model of a CCHP-CMG considering the higher-order uncertainty of renewables and loads is proposed.

### *A. p-box Model for Uncertain Renewables and Loads*

The *p*-box model combines the probability model and the interval model to describe the uncertain fluctuation characteristics of a random variable by the upper and lower bounds of its CDF curve [24], as shown in Fig. 2. If the type of probabilistic distribution function of an uncertain variable is

determined and the interval numbers are used to describe its distribution parameters, this type of *p*-box is called a parameterized *p*-box, which can be described as:

$$X^P=\{F_X(x,[\boldsymbol{\theta}])|[\boldsymbol{\theta}]=[\underline{\boldsymbol{\theta}},\overline{\boldsymbol{\theta}}]\} \tag{21}$$

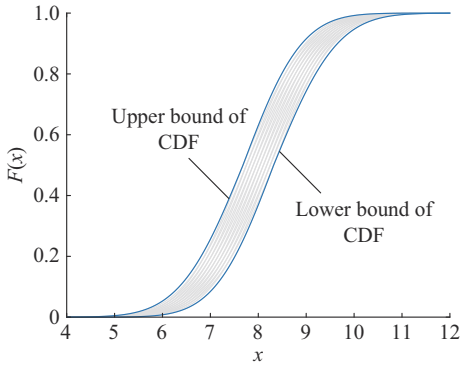


Fig. 2. Schematic diagram of *p*-box.

In the CCHP-CMG, the electricity/cooling/heating load power is assumed to obey the normal distribution, and its PDF $f_{\mathrm{WL}}(w_{\mathrm{L}})$ is shown as (22). Then, the *p*-box of the load power is expressed in the form as (23).

$$f_{\mathrm{WL}}(w_{\mathrm{L}})=\frac{1}{\sqrt{2\pi}\,\sigma_{\mathrm{L}}}\exp\left(-\frac{(w_{\mathrm{L}}-\mu_{\mathrm{L}})^2}{2\sigma_{\mathrm{L}}^2}\right) \tag{22}$$

$$W_{\mathrm{L}}^P=\{F_{\mathrm{WL}}(w_{\mathrm{L}},[\mu_{\mathrm{L}}],[\sigma_{\mathrm{L}}^2])|[\mu_{\mathrm{L}}]=[\underline{\mu}_{\mathrm{L}},\overline{\mu}_{\mathrm{L}}],[\sigma_{\mathrm{L}}^2]=[\underline{\sigma}_{\mathrm{L}}^2,\overline{\sigma}_{\mathrm{L}}^2]\} \tag{23}$$

Assuming that the solar irradiance obeys the Beta distribution, its PDF $f_{\mathrm{WR}}(w_{\mathrm{R}})$ is shown as (24) [25], [26].

$$f_{\mathrm{WR}}(w_{\mathrm{R}})=\frac{\Gamma(p_\alpha+p_\beta)}{\Gamma(p_\alpha)\Gamma(p_\beta)}(w_{\mathrm{R}}/w_{\mathrm{R,max}})^{p_\alpha-1}(1-w_{\mathrm{R}}/w_{\mathrm{R,max}})^{p_\beta-1} \tag{24}$$

The *p*-box model of $w_{\mathrm{R}}$ is expressed as follows:

$$W_{\mathrm{R}}^P=\{F_{\mathrm{WR}}(w_{\mathrm{R}},[p_\alpha],[p_\beta])|[p_\alpha]=[\underline{p}_\alpha,\overline{p}_\alpha],[p_\beta]=[\overline{p}_\beta,\underline{p}_\beta]\} \tag{25}$$

The PV and PT station outputs are calculated by $w_{\mathrm{R}}$:

$$\begin{cases}P_{\mathrm{PV}}=w_{\mathrm{R}}A_{\mathrm{PV}}\eta_{\mathrm{PV}}\\ Q_{\mathrm{PV}}=P_{\mathrm{PV}}\tan\theta_{\mathrm{PV}}\\ \Phi_{\mathrm{PT}}=w_{\mathrm{R}}A_{\mathrm{PT}}\eta_{\mathrm{PT}}\end{cases} \tag{26}$$

### *B. Chance Constraints of State Variable p-boxes*

When considering the higher-order uncertainty of the node power, the obtained state variables will also have higher-order uncertainty and can be described as *p*-boxes. Thus, the CCs of bus voltage *p*-box are described as (27). The probability $\Pr\{U_i\le U_{i,\max}\}$ is an interval instead of a definite value due to the *p*-box of bus voltage. To ensure the secure operation, the lower bound of the interval should be greater than the confidence level $\alpha_{U,\max}$. As shown in Fig. 3, the probability corresponding to point *A* requires to be greater than $\alpha_{U,\max}$. Similarly, the probability $\Pr\{U_{i,\min}\le U_i\}$ is also an interval, and the CC of the *p*-box requires the lower bound of this interval to be greater than the confidence level $\alpha_{U,\min}$.

$$\begin{cases}\inf(\Pr\{U_i\le U_{i,\max}\})\ge\alpha_{U,\max}\\ \inf(\Pr\{U_{i,\min}\le U_i\})\ge\alpha_{U,\min}\end{cases} \tag{27}$$

where inf(·) indicates obtaining the lower bound of an interval.

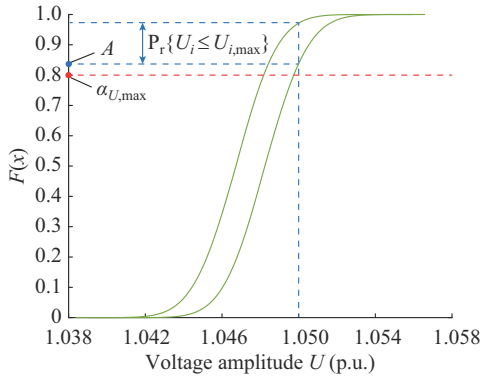


Fig. 3. Schematic diagram of *p*-box chance constraint.

The CCs of the *p*-boxes of pipeline mass flows and node supply temperatures can also be described as (28)-(30).

$$\begin{cases}\inf(\Pr\{m_{\mathrm{h/c}i}\le m_{\mathrm{h/c}i,\max}\})\ge\alpha_{\mathrm{mh/c,max}}\\ \inf(\Pr\{m_{\mathrm{h/c}i,\min}\le m_{\mathrm{h/c}i}\})\ge\alpha_{\mathrm{mh/c,min}}\end{cases} \tag{28}$$

$$\inf(\Pr\{T_{\mathrm{sh}i,\min}\le T_{\mathrm{sh}i}\})\ge\alpha_{\mathrm{Tsh,min}} \tag{29}$$

$$\inf(\Pr\{T_{\mathrm{sc}i}\le T_{\mathrm{sc}i,\max}\})\ge\alpha_{\mathrm{Tsc,max}} \tag{30}$$

### *C. Variance Constraints of State Variable p-boxes*

The variance of a random variable reflects its random fluctuation range. For the *p*-box of a state variable, each CDF curve corresponds to a variance value, and the variance of the *p*-box is an interval instead of a definite value. Thus, the random fluctuation range of the *p*-box is reflected by its variance interval. In the operation of CCHP-CMG, the state variable *p*-boxes are not only required to satisfy the secure CCs, but also required to reduce the random fluctuation ranges of state variables. The VCs of the voltage, mass flow, and supply temperature are as follows:

$$\begin{cases}0\le\mathrm{mid}([\sigma_{Ui}^2])\le\sigma_{U,\max}^2\\ 0\le\mathrm{mid}([\sigma_{\mathrm{mh}i}^2])\le\sigma_{\mathrm{mh,max}}^2\\ 0\le\mathrm{mid}([\sigma_{\mathrm{mc}i}^2])\le\sigma_{\mathrm{mc,max}}^2\\ 0\le\mathrm{mid}([\sigma_{\mathrm{Tsh}i}^2])\le\sigma_{\mathrm{Tsh,max}}^2\\ 0\le\mathrm{mid}([\sigma_{\mathrm{Tsc}i}^2])\le\sigma_{\mathrm{Tsc,max}}^2\end{cases} \tag{31}$$

Therefore, the proposed OEF model of a CCHP-CMG considering higher-order uncertainty is shown as:

$$\begin{cases}\min(C_{\mathrm{CCHP}}+C_{\mathrm{DN}})\\ \text{s.t. (4)-(15), (27)-(31)}\end{cases} \tag{32}$$

## IV. Solution Method for Proposed Model

For solving the optimization model (32), it is a critical and difficult task to transform the CCs and VCs of the state variable *p*-boxes to deterministic constraints. In this paper, the CCs and VCs of the *p*-boxes are transformed into constraints of various order cumulant intervals based on the *p*-efficient point theory and interval Cornish-Fisher expansion

method. And then, the IC method in [22] and affine algorithm are introduced to transform the CCs and the VCs of *p*-boxes into deterministic constraints.

### *A. Transformation of CCs and VCs of p-boxes*

The *p*-efficient point theory can be used to transform the CCs in the stochastic programming model into deterministic constraints [27]. A stochastic programming model with CCs is given as follows.

$$\begin{cases} \min\limits_{x} f(x) \\ \text{s.t. } \Pr\{g(x) \geq Z\} \geq p \\ \quad x \in X \end{cases} \tag{33}$$

The CDF of a random variable $Z$ is given as $F_Z(\boldsymbol{z}) = \Pr\{Z \leq \boldsymbol{z}\}$. Then, the $p$-level set is defined as $Z_p = \{\boldsymbol{z} \in \mathbf{R}^m : F_Z(\boldsymbol{z}) \geq p\}$, and thus, the stochastic programming model (33) can be rewritten as:

$$\begin{cases} \min\limits_{x} f(x) \\ \text{s.t. } g(x) \in Z_p \\ \quad x \in X \end{cases} \tag{34}$$

Let $p \in (0, 1)$, if $F_Z(z_p) \geq p$ and there is no point, $z \leq z_p$, $z \neq z_p$ such that $F_Z(z) \geq p$, then $z_p$ is called the $p$-efficient point of the CDF $F_Z(z)$. It is stated in [27] that if the random variable $Z$ is a scalar random variable, i.e., $m = 1$, the $p$-efficient point $z_p = F_Z^{-1}(p)$. If the $p$-efficient point $z_p$ of $Z$ is known, then from (34), the stochastic programming model (33) can be transformed into the following form.

$$\begin{cases} \min\limits_{x} f(x) \\ \text{s.t. } g(x) \geq z_p \\ \quad x \in X \end{cases} \tag{35}$$

Then, the CCs in (33) are transformed into deterministic constraints in (35). Thus, based on the *p*-efficient point theory, the CCs of the *p*-boxes of (27)-(30) can be transformed into the forms as follows:

$$\begin{cases} \sup(F_{Ui}^{-1}(\alpha_{U,\max})) \leq U_{i,\max} \\ \inf(F_{Ui}^{-1}(1-\alpha_{U,\min})) \geq U_{i,\min} \end{cases} \tag{36}$$

$$\begin{cases} \sup(F_{\text{mh/c}i}^{-1}(\alpha_{\text{mh/c},\max})) \leq m_{\text{h/c}i,\max} \\ \inf(F_{\text{mh/c}i}^{-1}(1-\alpha_{\text{mh/c},\min})) \geq m_{\text{h/c}i,\min} \end{cases} \tag{37}$$

$$\inf(F_{\text{Tsh}i}^{-1}(1-\alpha_{\text{Tsh},\min})) \geq T_{\text{sh}i,\min} \tag{38}$$

$$\sup(F_{\text{Tsh}i}^{-1}(\alpha_{\text{Tsc},\max})) \leq T_{\text{sc}i,\max} \tag{39}$$

The difficulty in the calculation of (36)-(39) is the solution of the inverse CDF functions, since the probability distribution models of PV/PT power outputs are all non-Gaussian. Thus, there is no deterministic probability distribution type for state variables, and the exact analytical expressions of the CDFs and the corresponding inverse functions for state variables cannot be obtained.

The calculation of the Cornish-Fisher expansion method can be found in [28]. Assume that the quantile of an output random variable $X$ is $\alpha$ $(0 < \alpha < 1)$, then, its corresponding value $x$ of the random variable can be expressed as:

$$x = c(\alpha) = \gamma_X^{(1)} + (\gamma_X^{(2)})^{\frac{1}{2}} \left\{ \zeta(\alpha) + \frac{\zeta^2(\alpha)-1}{6} g_3 + \frac{\zeta^3(\alpha)-3\zeta(\alpha)}{24} g_4 - \frac{2\zeta^3(\alpha)-5\zeta(\alpha)}{36} g_3^2 + \frac{\zeta^4(\alpha)-6\zeta^2(\alpha)+3}{120} g_5 + \cdots \right\} \tag{40}$$

$g_k$ can be obtained by:

$$g_k = \gamma_X^{(k)} / \sigma_X^k = \gamma_X^{(k)} / (\gamma_X^{(2)})^{\frac{k}{2}} \tag{41}$$

As observed from the above equation, the Cornish-Fisher expansion can be used to obtain the corresponding value of the random variable at a given quantile. Thus, the inverse CDF function $F_{Ui}^{-1}(\cdot)$, $F_{mhi}^{-1}(\cdot)$, $F_{mci}^{-1}(\cdot)$, $F_{Tshi}^{-1}(\cdot)$ and $F_{Tcsi}^{-1}(\cdot)$ in (36)-(39) can be calculated by the Cornish-Fisher expansion. Since the output random variables are *p*-boxes, the results of the inverse CDF functions of the output random variables with respect to a quantile are intervals; thus, the Cornish-Fisher expansion needs to be extended to the following interval Cornish-Fisher expansion for the transformation of the CCs of *p*-boxes:

$$[x] = [c(\alpha)] = [\gamma_X^{(1)}] + ([\gamma_X^{(2)}])^{\frac{1}{2}} \left\{ \zeta(\alpha) + \frac{\zeta^2(\alpha)-1}{6} [g_3] + \frac{\zeta^3(\alpha)-3\zeta(\alpha)}{24} [g_4] - \frac{2\zeta^3(\alpha)-5\zeta(\alpha)}{36} [g_3^2] + \frac{\zeta^4(\alpha)-6\zeta^2(\alpha)+3}{120} [g_5] + \cdots \right\} \tag{42}$$

$[g_k]$ can be obtained as:

$$[g_k] = [\gamma_X^{(k)}] / ([\sigma_X])^k = [\gamma_X^{(k)}] / ([\gamma_X^{(2)}])^{\frac{k}{2}} \tag{43}$$

The CCs of *p*-boxes as (36)-(39) can be transformed into the following forms by the interval Cornish-Fisher expansion.

$$\begin{cases} \sup([c(\alpha_{U,\max})]) \leq U_{i,\max} \\ \inf([c(1-\alpha_{U,\min})]) \geq U_{i,\min} \end{cases} \tag{44}$$

$$\begin{cases} \sup([c(\alpha_{\text{mh/c},\max})]) \leq m_{\text{h/c}i,\max} \\ \inf([c(1-\alpha_{\text{mh/c},\min})]) \geq m_{\text{h/c}i,\min} \end{cases} \tag{45}$$

$$\inf(c(1-\alpha_{\text{Tsh},\min})) \geq T_{\text{sh}i,\min} \tag{46}$$

$$\sup(c(\alpha_{\text{Tsc},\max})) \leq T_{\text{sc}i,\max} \tag{47}$$

Further, in the above optimization model, the 2nd-order ICs of random variables is their variance intervals, and thus, the VCs in (31) can be transformed into constraints on the central value of the 2nd-order ICs, as shown in (48).

$$\begin{cases} 0 \leq \text{mid}([\gamma_{Ui}^{(2)}]) \leq \sigma_{U,\max}^2 \\ 0 \leq \text{mid}([\gamma_{\text{mh}i}^{(2)}]) \leq \sigma_{\text{mh},\max}^2 \\ 0 \leq \text{mid}([\gamma_{\text{mc}i}^{(2)}]) \leq \sigma_{\text{mc},\max}^2 \\ 0 \leq \text{mid}([\gamma_{\text{Tsh}i}^{(2)}]) \leq \sigma_{\text{Tsh},\max}^2 \\ 0 \leq \text{mid}([\gamma_{\text{Tsc}i}^{(2)}]) \leq \sigma_{\text{Tsc},\max}^2 \end{cases} \tag{48}$$

### *B. Representation of Relationship Between ICs of State Variables and Node Power*

The IC method proposed in [22] is introduced to obtain the relationship between the ICs of state variables and node powers. Given that the $k^{\text{th}}$-order IC of the node power fluctuations

is $[\boldsymbol{\gamma}_{\Delta W}^{(k)}]$, the $k^{\text{th}}$-order IC of the state variable fluctuations can be obtained from the following equation.

$$[\boldsymbol{\gamma}_{\Delta X}^{(k)}]=\boldsymbol{S}^{\langle k\rangle}[\boldsymbol{\gamma}_{\Delta W}^{(k)}] \quad k\in\mathbf{N}^{+} \tag{49}$$

where $[\boldsymbol{\gamma}_{\Delta X}^{(k)}]=[[\boldsymbol{\gamma}_{\Delta U}^{(k)}];[\boldsymbol{\gamma}_{\Delta mh}^{(k)}];[\boldsymbol{\gamma}_{\Delta mc}^{(k)}];[\boldsymbol{\gamma}_{\Delta T\text{sh}}^{(k)}];[\boldsymbol{\gamma}_{\Delta T\text{sc}}^{(k)}]]$; $[\boldsymbol{\gamma}_{\Delta W}^{(k)}]=[[\boldsymbol{\gamma}_{\Delta P\text{e}}^{(k)}];[\boldsymbol{\gamma}_{\Delta Q\text{e}}^{(k)}];[\boldsymbol{\gamma}_{\Delta\Phi\text{h}}^{(k)}];[\boldsymbol{\gamma}_{\Delta\Phi\text{c}}^{(k)}]]$; and $\boldsymbol{S}^{\langle k\rangle}$ is the matrix composed of the $k^{\text{th}}$ power of each element in the sensitivity matrix $\boldsymbol{S}$. $[\boldsymbol{\gamma}_{\Delta W}^{(k)}]$ can be calculated from the probabilistic model and distribution parameters of the renewables and loads by the method in [22]. $[\boldsymbol{\gamma}_{\Delta U}^{(k)}]$, $[\boldsymbol{\gamma}_{\Delta mh}^{(k)}]$, $[\boldsymbol{\gamma}_{\Delta mc}^{(k)}]$, $[\boldsymbol{\gamma}_{\Delta T\text{sh}}^{(k)}]$, $[\boldsymbol{\gamma}_{\Delta T\text{sc}}^{(k)}]$ are the $k^{\text{th}}$-order IC vectors of the fluctuations of bus voltage, heating/cooling pipeline mass flow, and heating/cooling node supply temperature, respectively. The sensitivity matrix $\boldsymbol{S}$ can be obtained from the inverse of the Jacobi matrix. And the Jacobi matrix is calculated from the partial derivatives of the energy flow equation of the CCHP-CMG with respect to the state variables by substituting the values of the state variables in the optimal operation point. Hence, the components in the matrix $\boldsymbol{S}$ are associated with the decision variables.

Combined with the state variables $\boldsymbol{X}_0$ ($\boldsymbol{X}_0=[\boldsymbol{U}_0;\boldsymbol{m}_{\text{h}0};\boldsymbol{m}_{\text{c}0};\boldsymbol{T}_{\text{sh}0};\boldsymbol{T}_{\text{sc}0}]$) in the steady operation point corresponding to the expected values of random variables, the $k^{\text{th}}$-order ICs of state variables can be obtained as:

$$\begin{cases}[\boldsymbol{\gamma}_{X}^{(1)}]=[\boldsymbol{\gamma}_{\Delta X}^{(1)}]+\boldsymbol{X}_0\\ [\boldsymbol{\gamma}_{X}^{(k)}]=[\boldsymbol{\gamma}_{\Delta X}^{(k)}] \quad k\geq 2\end{cases} \tag{50}$$

where $[\boldsymbol{\gamma}_{X}^{(k)}]=[[\boldsymbol{\gamma}_{U}^{(k)}];[\boldsymbol{\gamma}_{m\text{h}}^{(k)}];[\boldsymbol{\gamma}_{mc}^{(k)}];[\boldsymbol{\gamma}_{T\text{sh}}^{(k)}];[\boldsymbol{\gamma}_{T\text{sc}}^{(k)}]]$ is the $k^{\text{th}}$-order IC vector of state variables.

### *C. Affine Interval Arithmetic Method*

There are lots of interval operations in the calculation of the CIs of state variables and the interval Cornish-Fisher expansion, and the above transformed optimization model is an interval optimization model. To deal with the interval extension problem that exists in interval arithmetic, the intervals are expressed as affine forms in the solution of the optimization model.

Assume that an uncertain variable $u\in[\underline{u},\overline{u}]$ is subject to $n$ independent noise symbols, and then, $u$ can be expressed in the following affine form [29], [30]:

$$\hat{u}=u_0+u_1\varepsilon_1+\ldots+u_n\varepsilon_n=\sum_{i=1}^{n}u_i\varepsilon_i \tag{51}$$

The affine form and interval of an uncertain variable are interconvertible. The interval form corresponding to (51) is:

$$\begin{cases}[\underline{u},\overline{u}]=[u_0-\xi,u_0+\xi]\\ \xi=\sum_{i=1}^{n}|u_i|\end{cases} \tag{52}$$

Given an interval form $[\boldsymbol{u}]$, let $u_0=(\underline{u}+\overline{u})/2$ and $u_1=(\overline{u}-\underline{u})/2$; then, the corresponding affine form is:

$$[\boldsymbol{u}]=[\underline{u},\overline{u}]\Rightarrow\hat{u}=u_0+u_1\varepsilon_1 \quad \varepsilon_1\in[-1,1] \tag{53}$$

When the affine arithmetic is used to deal with linear operations, if the affine numbers $\hat{u}=u_0+u_1\varepsilon_1$, $\hat{v}=v_0+v_1\varepsilon_1$, and the constant $C$ are given, the following equation is obtained according to the rules of affine arithmetic.

$$\begin{cases}C\hat{u}=Cu_0+Cu_1\varepsilon_1\\ \hat{u}\pm C=(u_0\pm C)+u_1\varepsilon_1\\ \hat{u}\pm\hat{v}=u_0\pm v_0+(u_1\pm v_1)\varepsilon_1\end{cases} \tag{54}$$

When the affine arithmetic is used to deal with nonlinear operations, new noise element is generated for each affine multiplication/division, and the partial derivative of the noise element is obtained by Chebyshev approximation or minimum range approximation [31], which may have approximation errors. Moreover, the accumulation of additional noise elements may lead to interval extension [32], and the additional noise elements also increase the complexity of solving the optimization model. Therefore, the nonlinear operations for affine forms are executed according to the following rules.

1) If the nonlinear function is monotonic, the central value and the 1st-order partial derivative of the output interval are calculated according to the monotonicity.

For example, the affine form of standard deviation $\hat{\sigma}_X$ of the state variable $X$ is calculated as follows:

$$\hat{\sigma}_X=\sigma_{X,0}+\sigma_{X,1}\varepsilon_1=\sqrt{\hat{\gamma}_X^{(2)}}=\sqrt{\gamma_{X,0}^{(2)}+\gamma_{X,1}^{(2)}\varepsilon_1} \tag{55}$$

Since the square root operation is monotonically increasing, $\sigma_{X,0}$ and $\sigma_{X,1}$ can be obtained by:

$$\begin{cases}\sigma_{X,0}=\sqrt{\gamma_{X,0}^{(2)}+\gamma_{X,1}^{(2)}}+\dfrac{1}{2}\sqrt{\gamma_{X,0}^{(2)}-\gamma_{X,1}^{(2)}}\\ \sigma_{X,1}=\sqrt{\gamma_{X,0}^{(2)}+\gamma_{X,1}^{(2)}}-\dfrac{1}{2}\sqrt{\gamma_{X,0}^{(2)}-\gamma_{X,1}^{(2)}}\end{cases} \tag{56}$$

2) If the nonlinear function is non-monotonic, the central value and the 1st-order partial derivative of the output interval are calculated based on the interval Taylor series expansion.

Given the interval function $[y]=f([\boldsymbol{u}])$, the first-order interval Taylor series expansion of the interval function $f([\boldsymbol{u}])$ at the central value of the interval $[\boldsymbol{u}]$, i.e., $\boldsymbol{u}_0$, is as (57) [33].

$$[y]=f([\boldsymbol{u}])=f(\boldsymbol{u}_0)+\sum_{k=1}^{m}\left.\frac{\partial f(\boldsymbol{u})}{\partial u_k}\right|_{\boldsymbol{u}=\boldsymbol{u}_0}([u_k]-u_{0k}) \tag{57}$$

where $u_k$ ($k=1,2,\ldots,m$) is the $k^{\text{th}}$ element in $\boldsymbol{u}$; and $u_{0k}$ is the $k^{\text{th}}$ element in $\boldsymbol{u}_0$.

Thus the 1st-order affine form of the output interval $\hat{y}=y_0+y_1\varepsilon_1$ can be obtained from:

$$\begin{cases}y_0=f(\boldsymbol{u}_0)\\ y_1=\sum_{k=1}^{m}\left|\left.\frac{\partial f(\boldsymbol{u})}{\partial u_k}\right|_{\boldsymbol{u}=\boldsymbol{u}_0}u_{k,1}\right|\end{cases} \tag{58}$$

where $u_{k,1}$ is the 1st-order partial derivative of the affine form of $u_k$.

Thus, in the optimization model, the intervals are transformed into affine forms according to (53) and calculated according to the rules shown in (54)-(58).

### *D. Transformed Deterministic Optimization Model*

In summary, the OEF model considering the higher-order uncertainty in (32) can be transformed into the form as (59). In this optimization model, all the intervals are transformed into affine forms according to (53)-(58). Therefore, the OEF model considering the higher-order uncertainty as (32) is

transformed into a deterministic optimization model, which can be efficiently solved by the CONOPT solver in the mature commercial optimization software GAMS [34].

$$\begin{cases} \min\left(C_{\mathrm{CCHP}}+C_{\mathrm{DN}}\right) \\ \text{s.t. (4)-(15), (44)-(50)} \end{cases} \tag{59}$$

## V. Case Study

### A. Structure and Parameters of CCHP-CMG

The structure of a CCHP-CMG is shown in Fig. 4, which is divided into two energy supply areas (Area I and Area II) with three energy stations.

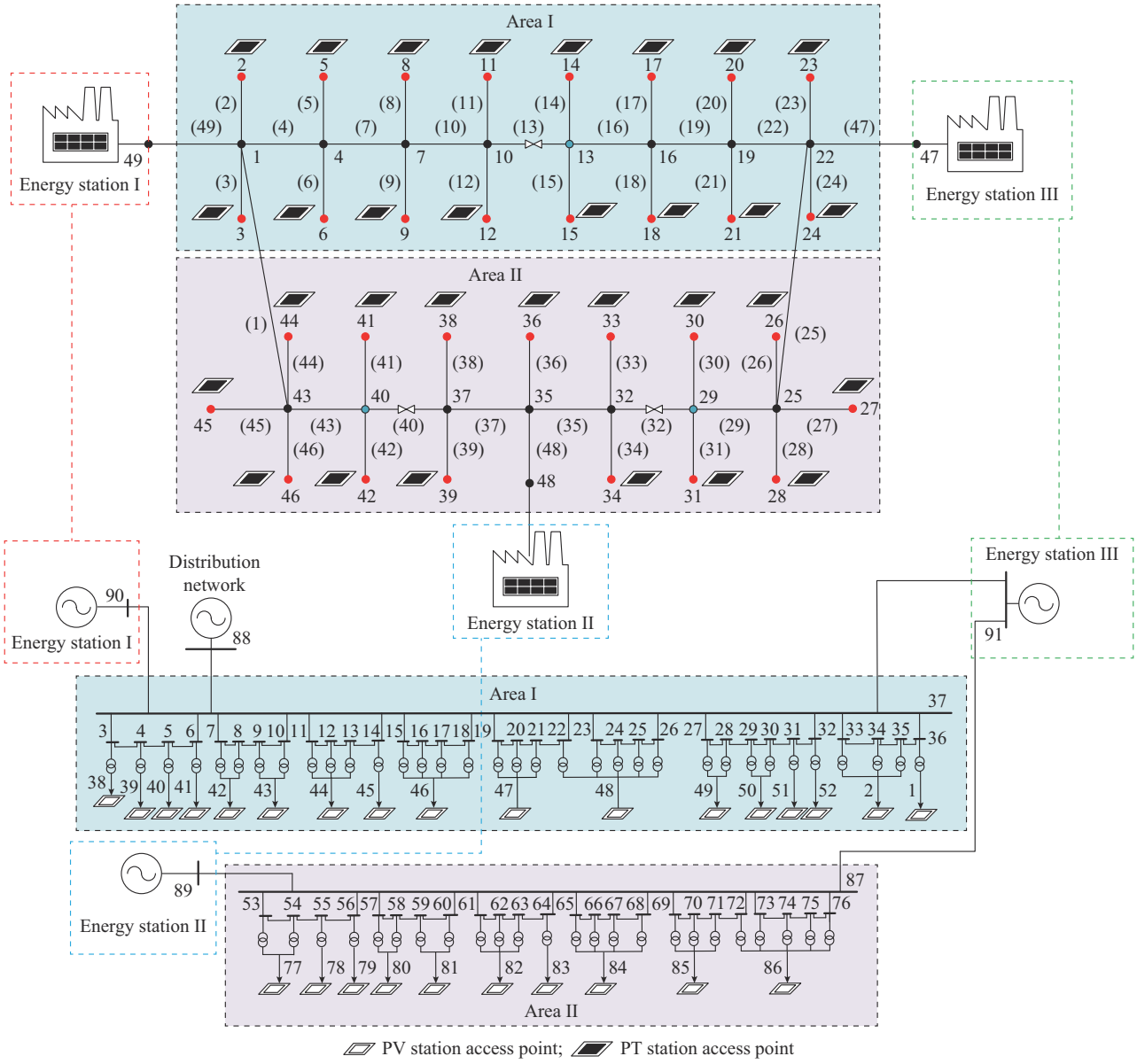


Fig. 4. Structure of CCHP-CMG.

The cooling and heating networks in the CCHP-CMG have the same structure, both including 49 nodes and 49 pipelines. Energy stations I, II, and III are located at nodes 49, 48, and 47, and energy stations II and III are the balancing nodes of heating and cooling network, respectively. The electricity network includes 91 buses, energy stations I-III are located at the buses 90, 89, and 91, respectively. The bus 88 connected to the public distribution network is set as the swing bus and its voltage is fixed at 1.05 p.u.. The generated electric power of the CCHP units in the energy stations I-III is determined by their heating power output. The PV and PT stations are connected to the load buses/nodes of the electricity and heating networks, respectively. The central values of the shape parameter intervals $[p_\alpha]$ and $[p_\beta]$ of the solar irradiance are given as 0.6798 and 1.7788 [18], respectively, and the radii of the intervals are given as 1.5% of the central values. The power output of the PV station at each electric load bus accounts for 15% of its electrical load power, and the power output of the PT station at each heating load node accounts for 5% of its heating load power [22]. The central values of the mean intervals $[\mu_{\mathrm{L}}]$ of the electricity/heating/cooling loads are given by the data in [22], the radius of the

mean interval is given as 1.5% of the central value, and the standard deviation interval $[\sigma_L]=5\%\cdot[\mu_L]$. The cost coefficients $a_{0i}$, $a_{1i}$, $a_{2i}$, $a_{3i}$, $a_{4i}$, $a_{5i}$ can be set as the values in [23], i.e., $a_{0i}$=¥1250, $a_{1i}$=0.6 ¥/kW, $a_{2i}$=0.027 ¥/kW$^2$, $a_{3i}$=14 ¥/kW, $a_{4i}$=0.0435 ¥/kW$^2$, and $a_{5i}$=0.011 ¥/kW$^2$. The unit power purchase price $c_{DN}$ is 1.0 ¥/kWh.

In the case study, the voltage regulation range of the CCHP unit is [1.05, 1.10]p.u. and the temperature regulation ranges are as follows: $T_{Gsi,h,min}=80$ ℃, $T_{Gsi,h,max}=90$ ℃, $T_{Gsi,c,min}=4$ ℃, $T_{Gsi,c,max}=8$ ℃. The secure limits of state variables are as follows: $U_{i,min}=0.95$ p.u., $U_{i,max}=1.05$ p.u., $m_{hi,min}=-15$ kg/s, $m_{hi,max}=15$ kg/s, $m_{ci,min}=-150$ kg/s, $m_{ci,max}=150$ kg/s, $T_{shi,min}=80$ ℃, and $T_{sci,max}=10$ ℃. In the CCs of *p*-boxes of state variables, the confidence levels for all CCs are given as 0.95. The used computer is a PC with an Intel Core i7-8700 CPU and 32 GB RAM. The optimization model is solved by the CONOPT solver in GAMS software, version GAMS win 64 23.9.5.

Four different methods are used for comparison, as shown in Table I.

TABLE I
MATHEMATICAL MODELS OF FOUR METHODS

| No. | Method | Equation |
|---|---|---|
| I | Proposed OEF considering the higher-order uncertainty | (32) or (59) |
| II | Deterministic OEF | (60) |
| III | Traditional CCP-based OEF | (20) |
| IV | IGDT-based OEF | (61) |

The deterministic OEF model is shown in (60). The IGDT-based OEF model is shown in (61) [35].

$$\begin{cases} \min\left(C_{CCHP}+C_{DN}\right) \\ \text{s.t. (4)-(15)} \\ \quad U_{i,\min}\le U_i\le U_{i,\max} \\ \quad m_{h/ci,\min}\le m_{h/ci}\le m_{h/ci,\max} \\ \quad T_{sh/ci,\min}\le T_{sh/ci}\le T_{sh/ci,\max} \end{cases} \tag{60}$$

$$\begin{cases} \max \alpha \\ \text{s.t. } f_{ob}\le f_{ob,0}\left(1+\delta_{ob}\right) \\ \quad f_{ob}=C_{CCHP}+C_{DN} \\ \quad \text{(2)-(15)} \\ \quad U_{i,\min}\le U_i\le U_{i,\max} \\ \quad m_{h/ci,\min}\le m_{h/ci}\le m_{h/ci,\max} \\ \quad T_{sh/ci,\min}\le T_{sh/ci}\le T_{sh/ci,\max} \\ \quad \boldsymbol{w}_L=(1+\alpha)\cdot\text{mid}([\boldsymbol{\mu}_L]) \\ \quad P_{PVi}=(1-\alpha)\cdot\text{mid}([P_{PVi}]) \\ \quad Q_{PVi}=(1-\alpha)\cdot\text{mid}([Q_{PVi}]) \\ \quad \boldsymbol{\Phi}_{PT}=(1-\alpha)\cdot\text{mid}([\boldsymbol{\Phi}_{PT}]) \end{cases} \tag{61}$$

where $\alpha$ is the maximum fluctuation range; $f_{ob}$ is the objective function; $f_{ob,0}$ is the base level of the objective function (obtained by deterministic OEF algorithm); and $\delta_{ob}$ is the acceptable level of the objective function.

### *B. Analysis of Results of Traditional CCP-based OEF*

The probability distribution parameters of random variables are taken as the central values of their given intervals, and the optimal operation point is obtained by solving the traditional CCP-based OEF model (20). With this optimal operation point, the upper and lower bounds of all the state variables under the probability models and the *p*-box models of node power random variables are calculated, respectively. For the heating/cooling network, the mass flows of the energy station output pipelines are significantly larger than those of the other pipelines, which are easier to exceed the upper limit. Thus, the following analysis focuses on the mass flow of the energy station output pipelines, i.e., pipes (47)-(49), and their fluctuation intervals are shown in Table II. Since the energy station II connected to the heating pipeline (48) is the heating network balance node, it bears the unbalanced power caused by the uncertain fluctuation of renewables and loads; hence, the mass flow of pipeline (48) is a fluctuation interval. While the energy stations connected to the heating pipelines (47) and (49) are the common source nodes of the heating network, their heating power outputs are control variables, hence, their mass flows are definite values and maintain constant in the uncertainty analysis. Similarly, for the cooling network, the mass flow of the pipeline (47) connected to the cooling network balance is a fluctuation interval, while the mass flows of the pipelines (48) and (49) connected to the common cooling source nodes are definite values. As observed in Table II, for the optimal operation point of the traditional CCP-based OEF, the mass flows of heating/cooling output pipes of the energy stations all satisfy the secure operation constraints. However, if the higher-order uncertainty is considered, the upper limit of the mass flow *p*-box of the heating pipe (48) is 15.70 kg/s, which exceeds the upper limit constraint (15 kg/s); and the upper limit of the mass flow *p*-box of the cooling pipe (47) is 153.80 kg/s, which exceeds the upper limit constraint (150 kg/s). Both are clearly at risk of exceeding the safe operation limits.

TABLE II
MASS FLOW BOUNDS OF HEATING AND COOLING PIPELINES CONNECTED TO ENERGY STATIONS OBTAINED BY PROBABILITY AND *P*-BOX MODELS

| Variable | Random model | Mass flow bound (kg/s) | | |
|---|---|---|---|---|
| | | (47) | (48) | (49) |
| $m_h$ | Probability | 10.52 | [11.54, 15.00] | 11.48 |
| | *p*-box | | [10.83, 15.70] | |
| $m_c$ | Probability | [142.33, 150.00] | 65.01 | 72.05 |
| | *p*-box | [138.53, 153.80] | | |

Similarly, the buses 47 and 49 of the electricity network have heavy loads, whose voltage amplitudes $U_{47}$ and $U_{49}$ have a higher risk of exceeding the limit. Thus, taking them as examples, their fluctuation intervals are shown in Table III. It can be observed that the fluctuation intervals of $U_{47}$ and $U_{49}$ obtained from the traditional chance constraint model satisfy the safety constraints. However, when the higher-order uncertainty is considered, the lower bounds of the *p*-boxes of $U_{47}$ and $U_{49}$ are 0.9481 and 0.9490, respectively, with the risk of exceeding the lower limit.

TABLE III
VOLTAGE AMPLITUDE BOUNDS OBTAINED BY PROBABILITY AND *P*-BOX MODELS

| Random model | Voltage amplitude bound (p.u.) | |
|---|---|---|
| | $U_{47}$ | $U_{49}$ |
| Probability | [0.9500, 0.9738] | [0.9509, 0.9642] |
| *p*-box | [0.9481, 0.9756] | [0.9490, 0.9769] |

Obviously, there are limitations in the traditional CCP-based OEF model because the higher-order uncertainties in the probabilistic model of uncertain variables are ignored, and thus the state variables may still have the risk of exceeding the limits when the uncertain distribution parameters of the renewables and loads are considered in the obtained optimal operation point. Therefore, it is necessary to consider the higher-order uncertainty of renewables and loads in the OEF calculation of the CCHP-CMG.

### *C. Analysis of OEF Calculation Results Considering Higher-order Uncertainty*

#### *1) OEF Calculation Results*

The upper limits of the variance intervals $\sigma^2_{U,\max}$ of the load bus voltages and the heating and cooling pipeline mass flows are given as $5.0\times10^{-5}$, 1.000, and 3.000, respectively. The optimal operation point obtained from the proposed OEF method considering higher-order uncertainty is compared with that obtained from the deterministic OEF method to reflect the control effect of the CCs and VCs of the *p*-boxes. Taking the cooling pipeline mass flow $m_{c47}$ as an example, given the *p*-boxes of solar irradiance and loads, the p-boxes of $m_{c47}$ corresponding to the optimal operation points obtained by the two methods are shown in Fig. 5. In the optimal operation point obtained by Method II, when considering the higher-order uncertainty of renewables and loads, the obtained *p*-box of $m_{c47}$ greatly exceeds the upper limit. However, the fluctuation range of the *p*-box of $m_{c47}$ corresponding to the optimal operation point obtained by Method I can satisfy the secure operation constraint, and the fluctuation range of the *p*-box is obviously reduced, i. e., the random fluctuation degree of the *p*-box is also reduced.

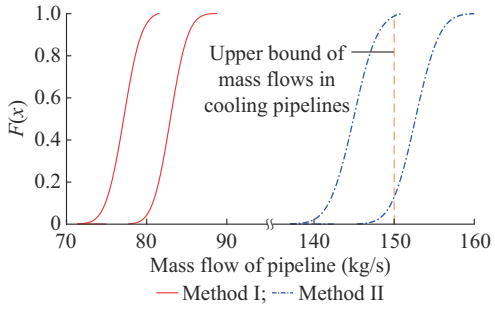


Fig. 5. *p*-boxes of $m_{c47}$ obtained by different methods.

In the optimal operation points obtained by Method I and Method II, considering the higher-order uncertainty of renewables and loads, the *p*-box bounds of mass flow of heating output pipes of the energy stations are shown in Table IV, and the central values and radii of their variance intervals are shown in Table V. It can be observed that in the results obtained from Method II, the upper bounds of the *p*-box fluctuation ranges of $m_{h48}$ and $m_{c47}$ are 16.19 kg/s and 156.55 kg/s, respectively, both exceeding the upper limits of secure operation. However, in the results obtained from Method I, the *p*-box fluctuation ranges of all the above variables can satisfy the secure operation constraints. Moreover, the central and radius values of the variance intervals of $m_{h48}$ and $m_{c47}$ by the Method I are significantly reduced, which can effectively reduce the fluctuation ranges of the *p*-boxes of $m_{h48}$ and $m_{c47}$.

TABLE IV
*P*-BOX BOUNDS OF MASS FLOW OF HEATING OUTPUT PIPES OF ENERGY STATIONS

| Method | Variable | Mass flow bound (kg/s) | | |
|---|---|---|---|---|
| | | (47) | (48) | (49) |
| I | $m_h$ | 10.19 | [8.22, 12.87] | 12.52 |
| | $m_c$ | [97.03, 108.50] | 41.58 | 69.03 |
| II | $m_h$ | 11.24 | [11.23, 16.19] | 10.88 |
| | $m_c$ | [141.13, 156.55] | 64.90 | 72.47 |

TABLE V
CENTRAL VALUES AND RADII OF VARIANCE INTERVALS OF *P*-BOXES OF $m_{h48}$ AND $m_{c47}$

| Method | $m_{h48}$ | | $m_{c47}$ | |
|---|---|---|---|---|
| | Central value | Radius | Central value | Radius |
| I | 1.000 | 0.019 | 3.000 | 0.045 |
| II | 1.149 | 0.022 | 5.543 | 0.083 |

Comparison of the *p*-box fluctuation ranges of the supply temperatures of the heating/cooling load nodes obtained by Method I and Method II are shown in Fig. 6 and Fig. 7, respectively. It can be observed that the *p*-boxes of supply temperature at some heating load nodes obtained from Method II have the risk of exceeding the lower limit, while the fluctuation ranges of the *p*-boxes of all supply temperatures obtained from Method I satisfy the given secure operation constraints. In addition, due to the heating load nodes are connected to the PT stations, the uncertain fluctuations of renewables lead to larger fluctuation ranges of supply temperature *p*-boxes at the heating node than those at the cooling nodes.

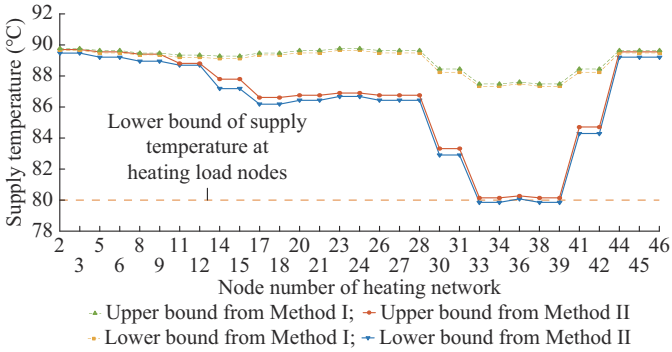


Fig. 6. *p*-box fluctuation bounds of supply temperature at heating load nodes.

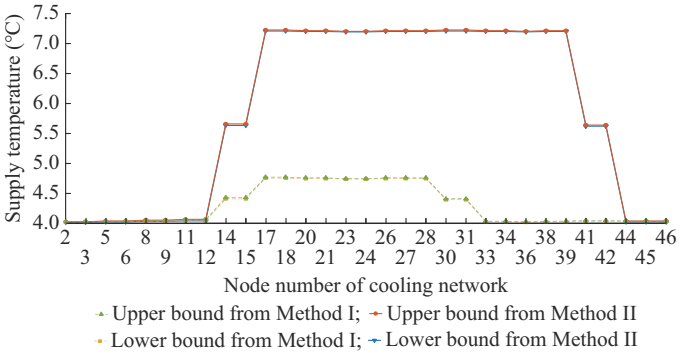


Fig. 7. *p*-box fluctuation bounds of supply temperature at cooling load nodes.

For the electricity network, in the optimal operation point obtained by Method I and Method II, the *p*-box fluctuation ranges of the load bus voltages are shown in Fig. 8, and the central values and radii of their variance intervals are shown in Fig. 9.

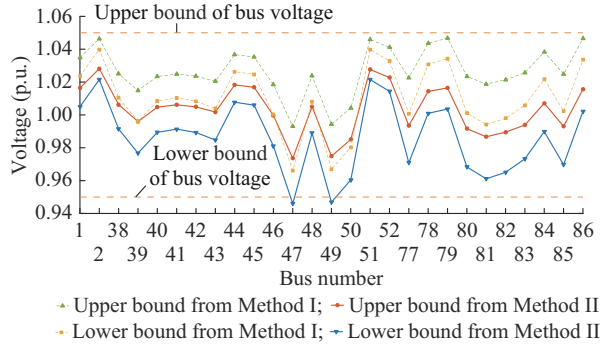


Fig. 8. *p*-box bounds of load bus voltages of electricity network.

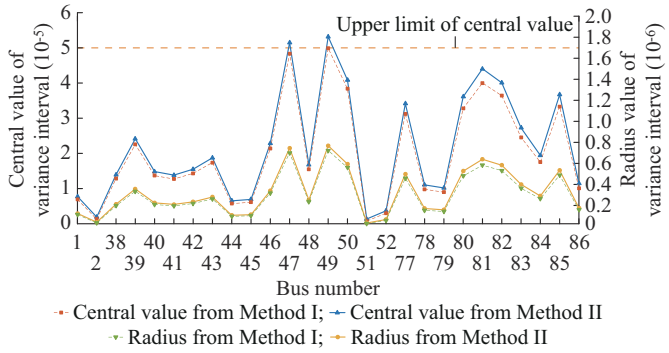


Fig. 9. Central values and radius values of variance intervals of *p*-boxes of load bus voltages.

It can be observed that the lower bounds of *p*-box fluctuation ranges of $U_{47}$ and $U_{49}$ (i.e., $U^{P}_{47,\mathrm{inf}}$ and $U^{P}_{49,\mathrm{inf}}$) corresponding to the optimal operation point obtained by Method II exceed the secure operation limits. However, for the optimal operation point obtained by Method I, the lower bounds of all the bus voltage *p*-boxes can satisfy the secure operation requirements ($U^{P}_{47,\mathrm{inf}}=0.9638$ p.u. and $U^{P}_{49,\mathrm{inf}}=0.9646$ p.u.); and the maximum upper bound of all the bus voltage *p*-boxes is 1.0467, which also satisfies the secure operation requirement. In addition, the central values and radii of variance intervals of bus voltages were reduced. Among them, the central values of variance intervals of $U_{47}$ and $U_{49}$ decrease from $5.10\times10^{-5}$ and $5.27\times10^{-5}$ to $4.84\times10^{-5}$ and $5.00\times10^{-5}$, respectively; and the radius values of variance intervals decrease from $7.45\times10^{-7}$ and $7.67\times10^{-7}$ to $6.94\times10^{-7}$ and $7.17\times10^{-7}$, respectively. Thus, the fluctuation ranges of the *p*-boxes of bus voltages are effectively reduced. Therefore, for Method I, which takes into account the higher-order uncertainty of renewables and loads, the obtained optimal operation point can ensure that the state variable *p*-boxes satisfy the secure operation requirements and their random fluctuation ranges are effectively reduced.

Comparisons of the output power and main control variables of the CCHP unit of each energy station are shown in the Table VI and Table VII, respectively.

TABLE VI
OUTPUT POWER OF CCHP UNITS OF ENERGY STATIONS

| Energy station | Active power (MW) | | Reactive power (Mvar) | | Heating power (MW) | | Cooling power (MW) | |
|---|---|---|---|---|---|---|---|---|
| | Method I | Method II | Method I | Method II | Method I | Method II | Method I | Method II |
| I | 2.026 | 2.014 | 1.089 | 0.893 | 2.134 | 2.225 | 3.135 | 3.011 |
| II | 1.350 | 1.403 | 5.657 | 1.612 | 2.117 | 2.334 | 1.395 | 1.314 |
| III | 1.900 | 1.812 | 2.700 | 1.898 | 2.625 | 2.280 | 2.315 | 2.430 |

TABLE VII
CONTROL VARIABLES FOR CCHP UNITS OF ENERGY STATIONS

| Energy station | Generator voltage (p.u.) | | Heating temperature (°C) | | Cooling temperature (°C) | |
|---|---|---|---|---|---|---|
| | Method I | Method II | Method I | Method II | Method I | Method II |
| I | 1.089 | 1.058 | 90.000 | 87.184 | 4.723 | 7.18 |
| II | 1.082 | 1.051 | 87.832 | 80.528 | 4.000 | 7.18 |
| III | 1.086 | 1.055 | 90.000 | 90.000 | 4.000 | 4.00 |

It can be observed that the optimization of the voltage magnitude *p*-boxes is performed by adjusting the reactive power output and the generator voltage. And the optimization of the mass flow *p*-boxes is achieved by adjusting the supply temperature of the CCHP unit. As can be observed from (8), by increasing the temperature difference between the supply temperature and the ambient temperature, the mass flow can be reduced to meet the requirement of its *p*-box constraint.

*2) Comparative Results with Other Methods*

The objective function value and the number of state variables exceeding the secure limits obtained by the four methods in Table I are shown in Table VIII, in which the acceptable level $\delta_{ob}$ is set to be 0.01 for Method IV. It can be observed that compared with the optimal operation points obtained by Method II and Method III, although the operation cost of the optimal operation point obtained by Method I is slightly increased, there is no risk of exceeding the secure limit for each state variable when considering the higher-order uncertainties of the renewables and loads, which can en-

sure the secure operation of the CCHP-CMG. For Method IV, the obtained operation cost is higher than that of Method I, and the obtained optimal operation point still cannot ensure the secure operation of the CCHP-CMG because it does not consider the higher-order uncertainty. Moreover, when considering the higher-order uncertainties of the renewables and loads, the random fluctuation ranges of the state variables of Method I can be reduced by 2.71%, 2.42%, and 25.12% compared with those of Methods II, III, and IV, respectively. Therefore, Method I can effectively obtain the optimal operation point which can ensure the secure operation of the CCHP-CMG considering higher-order uncertainty of renewables and loads.

TABLE VIII
OBJECTIVE FUNCTION VALUE AND NUMBER OF STATE VARIABLES OUT OF LIMITS OBTAINED BY DIFFERENT METHODS

| Method | Objective function value (¥/hour) | Number of state variables exceeding secure limits |
|---|---|---|
| I | 26567.61 | 0 |
| II | 26558.20 | 8 |
| III | 26560.34 | 4 |
| IV | 26823.84 | 2 |

### D. Impact of Degree of Higher-order Uncertainty

In the cases with different higher-order uncertainty degrees, the computational results of different methods are compared to further verify the effectiveness of the proposed method. The higher-order uncertainty degree is measured by using the interval width ratio $k_m/k_m = \text{rad}([\theta])/\text{mid}([\theta])$, where $\theta$ is the distribution parameter $(\mu_L, \sigma_L, p_\alpha, p_\beta)$ of a random variable, and rad(·) represents the radius of the interval. The OEF has been calculated by setting $k_m = 0.5\%$, 1%, 1.5%, 2%, and 2.5%, and the other calculation process is the same as Section V-III. Taking $U^P_{47,\text{inf}}$ and $U^P_{49,\text{inf}}$, and the upper bounds of the *p*-boxes of mass flows of the heating pipeline (48) and cooling pipeline (47) (i.e., $m^P_{\text{h48,sup}}$ and $m^P_{\text{c47,sup}}$) as examples, their calculation results of the optimal operation points obtained by Methods I, II, III considering different higher-order uncertainty degrees are shown in Table IX, and the corresponding radius values of the variance intervals are shown in Table X. It can be observed that the *p*-box bounds of the state variables obtained from Methods II and III exceed the secure limit in the cases with different higher-order uncertainty degrees. The bigger the higher-order uncertainty degree, the bigger the degree of exceeding the secure limit. However, the results obtained by Method I with different higher-order uncertainty degrees all satisfy the secure limit. In addition, the radius values of variance intervals of the state variable *p*-boxes corresponding to the optimal operation point obtained by Method I in all the cases are smaller than those corresponding to the optimal operation points obtained by Methods II and III. Therefore, the obtained optimal operation point of Method I in the cases with different higher-order uncertainty degrees can all satisfy the secure operation requirement.

TABLE IX
*P*-BOX BOUNDS OF SEVERAL STATE VARIABLES IN CASES WITH DIFFERENT DEGREES OF HIGHER-ORDER UNCERTAINTY

| $k_m$ (%) | Method | $U^P_{47,\text{inf}}$ | $U^P_{49,\text{inf}}$ | $m^P_{\text{h48,sup}}$ | $m^P_{\text{c47,sup}}$ |
|---|---|---|---|---|---|
| 0.5 | I | 0.9673 | 0.9681 | 12.41 | 106.56 |
| | II | 0.9472 | 0.9480 | 15.86 | 153.97 |
| | III | 0.9494 | 0.9502 | 15.24 | 151.27 |
| 1.0 | I | 0.9662 | 0.9670 | 12.87 | 108.50 |
| | II | 0.9460 | 0.9468 | 16.20 | 156.55 |
| | III | 0.9481 | 0.9490 | 15.71 | 153.80 |
| 1.5 | I | 0.9662 | 0.9670 | 12.87 | 108.50 |
| | II | 0.9460 | 0.9468 | 16.20 | 156.55 |
| | III | 0.9481 | 0.9490 | 15.71 | 153.80 |
| 2.0 | I | 0.9656 | 0.9664 | 13.10 | 109.48 |
| | II | 0.9454 | 0.9462 | 16.60 | 157.97 |
| | III | 0.9475 | 0.9483 | 15.95 | 155.07 |
| 2.5 | I | 0.9651 | 0.9659 | 13.33 | 110.45 |
| | II | 0.9448 | 0.9456 | 16.86 | 159.12 |
| | III | 0.9469 | 0.9477 | 16.18 | 156.34 |

TABLE X
RADIUS VALUES OF VARIANCE INTERVALS OF SEVERAL STATE VARIABLES IN CASES WITH DIFFERENT DEGREES OF HIGHER-ORDER UNCERTAINTY

| $k_m$ (%) | Method | rad($[\sigma_{U47}]$) | rad($[\sigma_{U49}]$) | rad($[\sigma_{\text{mh48}}]$) | rad($[\sigma_{\text{mc47}}]$) |
|---|---|---|---|---|---|
| 1 | I | $2.221\times10^{-7}$ | $2.292\times10^{-7}$ | 0.0061 | 0.0150 |
| | II | $2.341\times10^{-7}$ | $2.416\times10^{-7}$ | 0.0070 | 0.0277 |
| | III | $2.327\times10^{-7}$ | $2.402\times10^{-7}$ | 0.0067 | 0.0272 |
| 2 | I | $7.064\times10^{-7}$ | $7.293\times10^{-7}$ | 0.0193 | 0.0450 |
| | II | $7.447\times10^{-7}$ | $7.686\times10^{-7}$ | 0.0220 | 0.0831 |
| | III | $7.405\times10^{-7}$ | $7.643\times10^{-7}$ | 0.0212 | 0.0814 |
| 3 | I | $7.064\times10^{-7}$ | $7.293\times10^{-7}$ | 0.0193 | 0.0450 |
| | II | $7.447\times10^{-7}$ | $7.686\times10^{-7}$ | 0.0220 | 0.0831 |
| | III | $7.405\times10^{-7}$ | $7.643\times10^{-7}$ | 0.0212 | 0.0814 |
| 4 | I | $9.693\times10^{-7}$ | $1.001\times10^{-6}$ | 0.0263 | 0.0600 |
| | II | $1.022\times10^{-6}$ | $1.055\times10^{-6}$ | 0.0303 | 0.1298 |
| | III | $1.016\times10^{-6}$ | $1.049\times10^{-6}$ | 0.0291 | 0.1086 |
| 5 | I | $1.246\times10^{-6}$ | $1.287\times10^{-6}$ | 0.0337 | 0.0750 |
| | II | $1.314\times10^{-6}$ | $1.356\times10^{-6}$ | 0.0389 | 0.1386 |
| | III | $1.307\times10^{-6}$ | $1.349\times10^{-6}$ | 0.0372 | 0.1357 |

### E. Application of Proposed Method to Data of Multiple Time Periods

To further demonstrate the effectiveness of applying the proposed method to the cases of continuous fluctuations of renewables and loads, the data of continuous 2 hours in a day (8 time periods when one time period is 15 min) has been used to solve the proposed OEF model (59) of each time period. Assume that for the 8 time periods, the central values of $[\mu_L]$ are set to be (1.0, 1.01, 1.02, 0.95, 1.04, 0.97, 1.06, 0.90) and the values of $w_{R,\max}$ are set to be (1.0, 1.01, 1.02, 0.95, 1.04, 0.97, 1.06, 0.90), and the base value 1.0 of the first time period corresponds to the case with the $[\mu_L]$ and $w_{R,\max}$ values in Section V-I to Section V-F. Other parameters are set the same as the former subsections. The ob-

tained optimal operation points are compared with those obtained by Method II. Comparison of the *p*-box bounds of the voltage magnitude of bus 47 is shown in Fig. 10, and those of the supply temperature of heating load node 33 is shown in Fig. 11. It can be observed that although the given fluctuations of renewables and loads vary with time, the obtained optimal operation points of Method I can still satisfy the secure operation requirement of the CCHP-CMG. However, for the optimal operation points obtained from Method II, when the higher-order uncertainty is considered, the voltage magnitudes of several electric load buses and the supply temperatures of several heating load nodes may exceed the secure operation limits. These results can further demonstrate the effectiveness of Method II considering the higher-order uncertainty of renewables and loads.

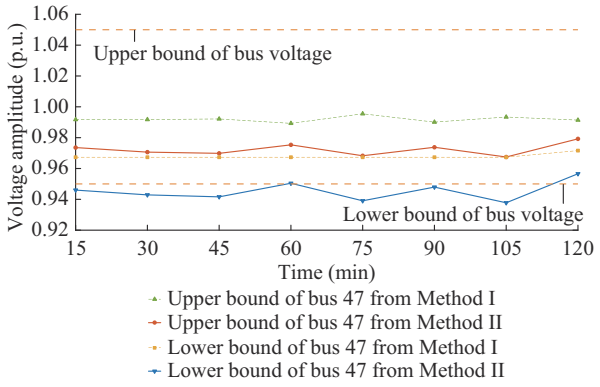


Fig. 10. *p*-box bounds of voltage magnitude of bus 47 in 2 hours of a day.

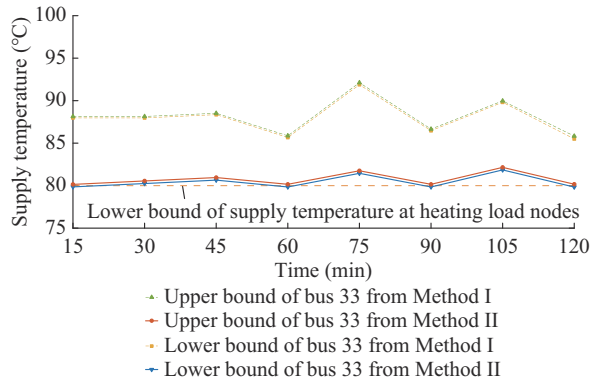


Fig. 11. *p*-box bounds of supply temperature of heating load node 33 in 2 hours of a day.

### *F. Comparison of Calculation Time*

Comparison of the calculation time of all the cases of different methods is shown in Table XI. In the solution of the proposed OEF model considering the higher-order uncertainty, the transformed deterministic nonlinear optimization problem can be efficiently solved by the commercial CONOPT solver, and it only consumes about 16.567 s. Although the calculation time of Method I is slightly increased compared with that of Methods II, III, and IV, the obtained optimal operation point can ensure the secure operation of the system when considering the higher-order uncertainty of renewables and loads, which is more suitable for application to the actual operation of the CCHP-CMG.

TABLE XI
COMPARISON OF CALCULATION TIME

| Method | Calculation time (s) |
|---|---|
| I | 16.567 |
| II | 7.486 |
| III | 8.628 |
| IV | 6.485 |

To verify the applicability considering the actual decision time frame for this CCHP-CMG application of Method I, we choose three different sizes of CCHP-CMGs as the case studies. The basic parameters and the consumed CPU time of the three cases are shown in Table XII. It can be observed that the larger the system size, the longer the consumed CPU time. However, Method I can obtain the optimal operation point of the system with less than 200 s, which can still satisfy the time frame requirements of the actual operation decision.

TABLE XII
BASE PARAMETERS AND CPU TIME OF THREE CASES

| Case | Number of cooling/heating network nodes and pipelines | Number of electricity network buses and branches | CPU time (s) |
|---|---|---|---|
| 1 | 13 and 12 | 54 and 78 | 4.275 |
| 2 | 49 and 49 | 91 and 136 | 16.567 |
| 3 | 72 and 73 | 126 and 192 | 159.659 |

## VI. CONCLUSION

In this paper, an OEF model of a CCHP-CMG considering the higher order uncertainty of renewables and loads is proposed. The CCs are used to describe the secure limits of the state variable *p*-boxes, and the VCs are introduced to reduce the random fluctuation ranges of the state variable *p*-boxes. In the solution of this model, the CCs and VCs of *p*-boxes are transformed into constraints of CIs of state variables based on the *p*-efficient point theory and interval Cornish-Fisher expansion. Then, with the relationship between the ICs of state variables and node power, and using the affine interval arithmetic method, the original OEF model is finally transformed into a deterministic nonlinear programming model, which can be solved by the CONOPT solver. Case study on a CCHP-CMG demonstrates that although the operation cost is only 0.0354% higher than that of the deterministic OEF, the obtained optimal operation point of the proposed OEF method can ensure the secure operation of the CCHP-CMG when considering the higher-order uncertainty of renewables and loads. The random fluctuation ranges of the state variables of the proposed OEF method can be reduced by 2.71%, 2.42%, and 25.12% compared with those of deterministic OEF, traditional CCP-based OEF, and IGDT-based OEF methods, respectively.

In the actual operation of a CCHP-CMG, there are correlation between different random variables of node power, and it will affect the OEF calculation results. Therefore, how to establish and solve the OEF calculation model considering the higher-order uncertainty and the correlation of multiple

random variables such as the correlation between different power outputs of renewable energy stations, is a possible direction of future work.

## REFERENCES


[1] J. Wu, J. Yan, H. Jia *et al*., "Integrated energy systems," *Applied Energy*, vol. 167, no. 1, pp. 155-157, Apr. 2016.

[2] W. Liang, S. Lin, S. Lei *et al.*, "Distributionally robust optimal dispatch of CCHP campus microgrids considering the time-delay of pipelines and the uncertainty of renewable energy," *Energy*, vol. 239, p. 122200, Jan. 2022.

[3] M. Mahmoodi, R. A. S. M. Noori, A. Attarha *et al.*, "Data-driven distributionally adjustable robust chance-constrained DG capacity assessment," *Journal of Modern Power Systems and Clean Energy*, doi: 10.35833/MPCE.2023.000029

[4] C. Wang, R. Gao, and W. Wei, "Risk-based distributionally robust optimal gas-power flow with Wasserstein distance," *IEEE Transactions on Power Systems*, vol. 34, no. 3, pp. 2190-2204, May 2019.

[5] L. Bai, F. Li, H. Cui *et al.*, "Interval optimization based operating strategy for gas-electricity integrated energy systems considering demand response and wind uncertainty," *Applied Energy*, vol. 167, pp. 270-279, Apr. 2016.

[6] D. Yang, C. Zhang, C. Jiang *et al.*, "Interval method based optimal scheduling of regional multi-microgrids with uncertainties of renewable energy," *IEEE Access*, vol. 9, pp. 53292-53305, Apr. 2021.

[7] J. Liu, C. Chen, Z. Liu *et al.*, "An IGDT-based risk-involved optimal bidding strategy for hydrogen storage-based intelligent parking lot of electric vehicles," *Journal of Energy Storage*, vol. 27, p. 101057, Feb. 2020.

[8] S. Zhang, S. Ge, H. Liu *et al.*, "A multi-objective chance-constrained information-gap decision model for active management to accommodate multiple uncertainties in distribution networks," *Journal of Modern Power Systems and Clean Energy*, vol. 11, no. 1, pp. 17-34, Jan. 2023.

[9] A. Soroudi, "Taxonomy of uncertainty modeling techniques in renewable energy system studies," in *Large Scale Renewable Power Generation*, New York: Springer, 2014, pp. 1-17.

[10] A. Soroudi and T. Amraee, "Decision making under uncertainty in energy systems: state of the art," *Renewable and Sustainable Energy Reviews*, vol. 28, pp. 376-384, Dec. 2013.

[11] Y. Li, Y. Zou, Y. Tan *et al.*, "Optimal stochastic operation of integrated low-carbon electric power, natural gas, and heat delivery system," *IEEE Transactions on Sustainable Energy*, vol. 9, no. 1, pp. 273-283, Jan. 2018.

[12] M. Qadrdan, J. Wu, N. Jenkins *et al.*, "Operating strategies for a GB integrated gas and electricity network considering the uncertainty in wind power forecasts," *IEEE Transactions on Sustainable Energy*, vol. 5, no. 1, pp. 128-138, Jan. 2014.

[13] Y. Li, B. Wang, Z. Yang *et al.*, "Optimal scheduling of integrated demand response-enabled community-integrated energy systems in uncertain environments," *IEEE Transactions on Industry Applications*, vol. 58, no. 2, pp. 2640-2651, Apr. 2021.

[14] F. Qi, M. Shahidehpour, Z. Li *et al.*, "A chance-constrained decentralized operation of multi-area integrated electricity-natural gas systems with variable wind and solar energy," *IEEE Transactions on Sustainable Energy*, vol. 11, no. 4, pp. 2230-2240, Oct. 2020.

[15] J. Weinstein and M. Yildiz, "Impact of higher-order uncertainty," *Games and Economic Behavior*, vol. 60, no. 1, pp. 200-212, Jul. 2007.

[16] P. E. Lehner, K. B. Laskey, and D. Dubois, "An introduction to issues in higher order uncertainty," *IEEE Transactions on Systems, Man and Cybernetics Part A – System and Humans*, vol. 26, no. 3, pp. 289-293, May 1996.

[17] M. Lubin, Y. Dvorkin, and S. Backhaus, "A robust approach to chance constrained optimal power flow with renewable generation," *IEEE Transactions on Power Systems*, vol. 31, no. 5, pp. 3840-3890, Sept. 2016.

[18] Y. Zhang, S. Shen, and J. L. Mathieu, "Distributionally robust chance-constrained optimal power flow with uncertain renewables and uncertain reserves provided by loads," *IEEE Transactions on Power Systems*, vol. 32, no. 2, pp. 1378-1388, Mar. 2017.

[19] X. Lu, K. W. Chan, S. Xia *et al.*, "Security-constrained multiperiod economic dispatch with renewable energy utilizing distributionally robust optimization," *IEEE Transactions on Sustainable Energy*, vol. 10, no. 2, pp. 768-779, Apr. 2019.

[20] C. He, X. Zhang, T. Liu *et al.*, "Distributionally robust scheduling of integrated gas-electricity systems with demand response," *IEEE Transactions on Power Systems*, vol. 34, no. 5, pp. 3791-3803, Sept. 2019.

[21] X. Liu, J. Wu, N. Jenkins *et al.*, "Combined analysis of electricity and heat networks," *Applied Energy*, vol. 162, pp. 1238-1250, Jan. 2016.

[22] Y. Xie, S. Lin, W. Liang *et al.*, "Interval probabilistic energy flow calculation of CCHP campus microgrid considering interval uncertainties of distribution parameters," *IEEE Access*, vol. 8, pp. 141358-141372, Aug. 2020.

[23] Z. Li, W. Wu, M. Shahidehpour *et al.*, "Combined heat and power dispatch considering pipeline energy storage of district heating network," *IEEE Transactions on Sustainable Energy*, vol. 7, no. 1, pp. 12-22, Jan. 2016.

[24] Z. Xiao, X. Han, C. Jiang *et al.*, "An efficient uncertainty propagation method for parameterized probability boxes," *Acta Mechanica*, vol. 227, no. 3, pp. 633-649, Mar. 2016.

[25] M. Fan, V. Vittal, G. Heydt *et al.*, "Probabilistic power flow studies for transmission systems with photovoltaic generation using cumulants," *IEEE Transactions on Power Systems*, vol. 27, no. 4, pp. 2251-2261, Nov. 2012.

[26] S. Karaki, R. Chedid, and R. Ramadan, "Probabilistic performance assessment of autonomous solar-wind energy conversion systems," *IEEE Transactions on Energy Conversion*, vol. 14, no. 3, pp. 766-772, Sept. 1999.

[27] A. Shapiro, D. Dentcheva, and A. Ruszczynski, *Lectures on Stochastic Programming: Modeling and Theory*. Philadelphia: Society for Industrial Mathematics, 2009.

[28] S. R. Jaschke. (2001, Jul.). The Cornish-Fisher-expansion in the context of Delta-Gamma-Normal approximations. [Online]. Available: http://econpapers.repec.org/scripts/redir.pf?u=http%3A%2F%2Feconstor.eu%2Fbitstream%2F10419%2F62681%2F1%2F725393866.pdf;h=repec:zbw:sfb373:200154

[29] L. H. de Figueiredo and J. Stolfi, "Affine arithmetic: concepts and applications," *Numerical Algorithms*, vol. 37, no. 1, pp. 147-158, Dec. 2004.

[30] J. L. Stolfi and L. H. de Figueiredo, "An introduction to affine arithmetic," *TEMA (São Carlos)*, vol. 4, no. 3, pp. 297-312, Dec. 2003.

[31] J. Luiz, D. Comba, and J. Stolfi, "Affine arithmetic and its applications to computer graphics," *Proceedings of VI SIBGRAPI*, vol. 1994, pp. 9-18, Jul. 1994.

[32] Y. Xie, S. Lin, W. Liang *et al.*, "An interval probabilistic energy flow calculation method for CCHP campus microgrids," *IEEE Systems Journal*, vol. 16, no. 4, pp. 6219-6230, Dec. 2022.

[33] R. E. Moore, R. B. Kearfott, and M. J. Cloud, *Introduction to Interval Analysis*. Philadelphia: Society for Industrial and Applied Mathematics, 2009.

[34] GAMS Development Corporation. (2010, Dec.). GAMS: the solver manuals. [Online]. Available: https://www. gams. com/latest/docs/S_MAIN.html

[35] M. Komeili, P. Nazarian, A. Safari *et al.*, "Robust optimal scheduling of CHP-based microgrids in presence of wind and photovoltaic generation units: an IGDT approach," *Sustainable Cities and Society*, vol. 78, p. 103566, Mar. 2016.



**Shunjiang Lin** received the B.S. degree in electrical engineering from the South China University of Technology, Guangzhou, China, in 2003, and the Ph. D. degree in electrical engineering from Hunan University, Changsha, China, in 2008. He is currently working as an Associate Professor in the School of Electric Power Engineering, South China University of Technology. His research interests include optimal operation and control of power systems and integrated energy systems.

**Xuan Sheng** received the B.S. degree in electrical engineering from the South China University of Technology, Guangzhou, China, in 2022. He is currently pursuing the M.S. degree in electrical engineering in South China University of Technology. His research interests include uncertainty analysis and optimization of integrated energy systems.

**Yuquan Xie** received the B.S. and M.S. degrees in electrical engineering from the South China University of Technology, Guangzhou, China, in 2019 and 2022, respectively. He is currently working as an Engineer in the Digital Grid Research Institute, China Southern Power Grid, Guangzhou, China. His research interests include uncertainty analysis and optimization of integrated energy systems.

**Yanghua Liu** received the Ph.D. degree in electrical engineering from Hu-

nan University, Changsha, China, in 2010. She is currently working as a Lecturer in the School of Electromechanical Engineering, Guangdong Polytechnic Normal University, Guangzhou, China. Her research interests include optimal operation and control of power systems and electricity market.

**Mingbo Liu** received the B.S. degree from Huazhong University of Science and Technology, Wuhan, China, in 1985, the M.S. degree from the Harbin Institute of Technology, Harbin, China, in 1988, and the Ph.D. degree from Tsinghua University, Beijing, China, in 1992. He is currently working as a Professor in the South China University of Technology, Guangzhou, China. He has authored or coauthored four monographs, two standards, and more than 280 articles. His research interests include energy management and operation control of power systems.